ORIGINAL ARTICLE

In-plane cyclic tests of strengthened rubble stone masonry

M. Ponte (iD) · **A. Penna** · **R. Bento**

Abstract This paper focuses on the in-plane behaviour of rubble stone masonry with lime mortar strengthened with different solutions. For that, 12 rubble stone masonry wall specimens, with construction features typical of ancient historic buildings of Southern Portugal and Mediterranean countries, were subjected to in-plane quasi-static cyclic tests. The applied retrofit solutions are specific for historic masonry buildings, such as the injection of mortar and FRCM systems, with glass and carbon meshes. The main experimental results obtained are presented through envelope curves, in terms of resistance, deformation capacity, and deformed shapes. Moreover, dissipated energy is also commented on. Horizontal drift results are compared and analysed together with the ones obtained in the literature for equivalent strengthening solutions in masonry walls.

1 Introduction

Past events have proved how existing masonry buildings are easily vulnerable to seismic action, either residential or monumental buildings (e.g. [1–4]). It is even worse when these buildings, due to the ageing process and little maintenance care, lack transversal connections or present poor masonry quality, in which diagonal shear cracks tend to appear in mortar joints because of its low tensile strength [5–8]. In fact, when the mortar is of very poor quality, it is very common to occur disintegration of the masonry or multiple-leaf separation phenomena under seismic events [9–11].

For the retrofitting of historic masonry structures, there is a combination of requirements to protect the authenticity of the cultural heritage building suggested by ICOMOS recommendations [12]. It states that the retrofit solutions must preserve the authenticity of the monument, promote minimum intervention, be reversible, where possible, and ensure compatibility and durability. Indeed, the requirement of reversibility can be discussed and questioned since there are very few truly reversible techniques. Therefore, the focus when

M. Ponte (✉) · R. Bento
Civil Engineering Research and Innovation for
Sustainability (CERIS), Instituto Superior Técnico (IST),
Universidade de Lisboa, Av. Rovisco Pais, Lisbon,
Portugal
e-mail: madalenaponte@tecnico.ulisboa.pt

R. Bento
e-mail: rita.bento@tecnico.ulisboa.pt

A. Penna
Department of Civil Engineering and Architecture,
University of Pavia, Via Ferrata 3, Pavia, Italy
e-mail: andrea.penna@unipv.it

designing the solutions should be instead on choosing compatible materials that can guarantee the efficiency and durability of the intervention, as stated by Oliveira et al. [13]. One of the most commonly used techniques is the grout injection of masonry walls, which exploits the existence of voids, significantly increasing the masonry mechanical properties (e.g. [14, 15]). However, its effectiveness depends on the injectability of the wall and the grout used [6, 16, 17]. In the past, some examples of misuse of this technique have been reported [18], mainly due to the application of incompatible materials such as cement-based mixtures in ancient buildings with a lime mortar substrate.

Another technique that has been recently increasingly investigated for improving the in-plane capacity of masonry walls is the Fabric Reinforced Cementitious Matrix (FRCM) system. The composites (either with glass, carbon, PBO, or even basalt meshes) present high compatibility with the masonry substrate and durability within the retrofit design, making them so attractive. Furthermore, for heritage masonry buildings, the inorganic matrix used should be lime-based mortars and not cement-based binders. At the moment, to the best of the authors' knowledge, these new materials are encoded for design in the USA [19] and, more recently, in Italy [20–24]. It is also worth mentioning the RILEM [24] and ACI [25] guidelines that exist on the subject. However, none of these codes or guidelines presents reference values for the increase of displacement capacity of strengthened walls, essential for the design of retrofitting solutions. As these materials are more recent, the existing relevant information on FRCM applied to historic masonry buildings is still scarce and some uncertainties regarding the design of the retrofit solution are still present. A recent paper by Boem [26] presents a review of masonry elements strengthened with this technique, showing several experimental works already developed. Most of the existing studies present FRCM systems applied on both facades of the specimens, but only a few exist with the strengthening on one side [27–31]. Furthermore, the existing studies on FRCM applied to rubble stone masonry carry out diagonal compression tests [30, 32–35], which provide data on improved equivalent tensile strength of masonry. Still, little information exists on cyclic behaviour and wall deformation capacity. The studies found by the authors on rubble stone walls strengthened with FRCM systems under in-plane quasi-static tests are [36–38].

As pointed out by Boem [26], studies in the literature have found that masonry piers strengthened with FRCM solutions and with a cantilever scheme tend to present flexural failure with toe crushing and without relevant diagonal cracks [39–41]. As noted from these tests, the effect of the proper anchoring of the FRCM system to the pier can often end in failure mechanisms ruled by rocking. On the other side, for tests with double fixed conditions, diagonal cracking, associated with a shear failure, typically rules the piers' behaviour [42, 43]. For more results on other boundary conditions, Petry and Beyer [44] have carried out several tests on unreinforced masonry walls under in-plane quasi-static loads.

The use of these two strengthening techniques, mortar injection and application of the FRCM system with FRP (fibre-reinforced polymers) meshes based on glass or carbon fibres, is herein investigated for the in-plane capacity improvement of rubble limestone masonry panels, typical of ancient constructions in Central-Southern Portugal.

For this purpose, an experimental program consisting of twelve rubble stone masonry specimens tested under quasi-static cyclic horizontal loads combined with constant vertical stress was developed. The experimental campaign was carried out in the Structures and Strength of Materials Laboratory (LERM) of the Instituto Superior Técnico (IST), University of Lisbon, within a partnership between IST and the SECIL Lda. Company. The experimental results were analysed to understand the change of behaviour of rubble stone walls when strengthened with different techniques, mainly the increase of displacement capacity, on which there are still almost no reference values available in the literature.

2 Experimental program

2.1 Specimens details

Twelve $120 \times 120 \times 40$ cm^3 specimens of rubble-stone masonry representative of ancient Portuguese monuments were built to assess their behaviour under quasi-static cyclic shear tests. Two unreinforced masonry (URM) walls were used as control, while the other specimens were strengthened with different solutions: mortar injection and FRCM system. Each combination of strengthening techniques was tested in

Table 1 Specimens' designation

Strengthening technique	Specimen designation
No Strengthening	URM 1, URM 2
Injection	I 1, I 2
FRCM system	
Glass-FRP mesh	G 1, G 2
Carbon-FRP mesh	C 1, C 2
Injection + FRCM system	
Glas-FRPs mesh	IG 1, IG 2
Carbon-FRP mesh	IC 1, IC 2

two specimens, giving a total of ten strengthened walls. The FRCM system was applied only on one side of the specimens, as is the case of many historic buildings due to architectural or conservation constraints, for instance, the presence of mural paintings or tiles on the walls, or when it is important to reduce the impact of the technique´s application in the building's use. The designation adopted for the specimens is presented in Table 1.

The specimens were built to reproduce the current condition of ancient masonry in Portuguese monuments and existing buildings. Thus, to represent the mortar's ageing effect, during the specimens' construction the interior core of the walls was left with several voids and only after a minimum period of 4 months after their construction they were tested, guaranteeing the mortar's curing. Moreover, the specimens were composed of two leaves of stone with occasional interlocking through the thickness, as shown in Fig. 1. The masonry units were irregularly shaped, with various dimensions, presenting an irregular texture typical of the ancient masonry buildings and monuments in the centre-south region of Portugal.

The specimens were built directly on reinforced concrete footings with dimensions $0.5 \times 1.25 \times 0.10$ m^3. A reinforced concrete beam with $0.5 \times 1.25 \times 0.10$ m^3 was built on top of each specimen to distribute the loads applied during the experimental tests.

When the walls were dry (minimum 28 days), the strengthening solutions were applied. Surface voids were sealed in all specimens with the same premixed mortar used in the construction to prevent injected mortar from being poured out of the walls in the specimens strengthened using such a technique.

The injection technique was applied through gravity as recommended for ancient deteriorated walls. The mortar was injected from a height of approximately 5 m higher than the specimens to obtain the necessary pressure (Fig. 2a), using an average of 3.7 bags of 18 kg of premixed mortar per panel. Four to five injection holes spaced approximately 50 cm apart with a light downward inclination were made on one side of each specimen. The injection holes were first filled with small quantities of water to clean the tubes and holes of small sediments and dust. Twenty-eight days after sealing the surface voids, the mortar was injected into the plastic tubes until it started to come out either from the same or other tubes, which were then closed (Fig. 2b). In the case of specimen I 1, as the tubes became filled with very little mortar injected, a total of 10 holes in different positions were made (Fig. 2c). However, even so, only a small quantity of mortar was injected, meaning the wall presented one of the lowest quantities of voids (3%). The percentage of voids was calculated and ranged between approximately 2% and 8%, with an average value of 5%.

The application of the FRCM systems (see Fig. 3), including its anchoring system, was applied following the CNR-DT 215/2018 guidelines [20] and the studies of Gattesco et al. [36]. Only one layer of mesh was applied and just on one side of the masonry specimens. The connectors for the glass mesh system, made of polypropylene and with an interior nail of glass-fibre reinforced polyamide, were applied by pressure, together with a further localised second layer of denser glass mesh (openings—5 × 5 mm) at the intersection of each connector with the Glass-FRP (GFRP) mesh, that helps to distribute the concentrated stresses generated around the connectors. Whereas the connectors used with the Carbon-FRP (CFRP) mesh already present a shape that allows a suitable distribution for peak stress. Both devices present a 10–15 cm anchorage length, which means they do not connect the two leaves of stone. Five connectors per wall were applied in 10 mm diameter holes drilled in the stones, with approximately 50 cm distance in between. No mechanical devices were applied to fix the ends of the FRP meshes to the concrete footing or top beam. The lack of continuity of the FRCM system at the ends of the masonry structural element is not in accordance with the good practices for the proper installation of the retrofitting technique that ensure the behaviour of the strengthening solution is fully exploited.

Fig. 1 Construction of the masonry specimens at LERM, IST

Fig. 2 Injection of specimen: **a** bucket and hose with mortar during injection, placed at 5 m height, **b** I 2 (pouring mortar from one of the lower tubes), and **c** I 1 (with several injection holes)

Fig. 3 Connectors applied to glass (left) and carbon (right) FRCM systems

Unfortunately, in heritage buildings, it is not often possible to fix the ends of the solution to the foundation or rooftop. Therefore, the authors decided to study this limitation.

The average thickness of the FRCM systems applied is around 20 mm, excluding the levelling of the substrate. To accommodate the high irregularities existent on the masonry surface of the specimens, the levelling layer thickness range is between 10 and 50 mm, and is made of the same matrix material as the FRCM system. Furthermore, the mesh was directly embedded in the levelling layer.

2.2 Mechanical characterization of materials

The specimens were built with roughly cut limestones, the most common stone used in ancient monuments and buildings surrounding Lisbon, from a quarry in "Porto-de-Mós". Compressive tests were carried out on stone cubic samples of about 50 mm edge length, following EN 1926 standard [45], and an average value of compressive strength of approximately 50 MPa was obtained, typical of a Portuguese soft limestone [46, 47].

The mortars applied for the construction and strengthening techniques were all based on premixed natural hydraulic lime mortars, compatible with historical buildings. The mortars used for building the masonry walls, fixing the FRP meshes to the substrate and the injection technique are here named A, B, and C, respectively. They were tested first to bending and then compression according to the EN 1015-11:2019 standard [48] for a minimum of 28 days of curing, using three specimens per mortar of the same batch with dimensions of $40 \times 40 \times 160$ mm each. Furthermore, three other specimens from the same previous batch of mortar A, used for the construction of the masonry walls, were also tested to bending and compression at 4 months old, the same mortar's age at which the cyclic tests started to be performed. Since the retrofitting techniques were later applied to the walls, the mortars used in the retrofitting were 30 days old when the quasi-static tests were carried out, similar to the age at which the mortars were mechanically characterized. The mortars' characterization for compression and flexural behaviour is presented in Table 2.

Regarding the application of the FRCM systems, the FRP meshes used were bidirectional, with glass or carbon fibres impregnated in the resin. The GFRP mesh, made of alkali-resistant glass fibres, due to the induction of resin with zirconia, presents a 40×40 mm^2 grid spacing, a mass per unit area of 38 g/m^2 for the longitudinal direction and 65 g/m^2 for the transversal, and resists, respectively, a tensile strength of 1720 and 3200 N/mm^2, according to the data provided by the manufacturer. It also presents Young's modulus larger than 55 GPa and ultimate tensile strain of 3.1 and 4.0% for the longitudinal and transversal directions, respectively. The CFRP mesh, made of carbon fibres bonded to an amorphous silica coating, presents a geometry with a grid spacing of 17×17 mm^2 and a mass per unit area of 374 g/m^2. According to the product technical forms, the CFRP mesh tensile strength is larger than 4300 N/mm^2, Young's modulus is 240 GPa, and presents an ultimate tensile strain of 1.8% for each direction. Both meshes were chosen between the available products on the Portuguese market in terms of dimensions and weight.

Compression tests were also carried out in three small masonry prisms with dimensions of $0.4 \times 0.4 \times 0.6$ m^3, as presented in Fig. 4a. The capacity curves of each prism during compression tests are presented in Fig. 4b in terms of vertical force and average vertical displacement (measured in four points, from the base footing to the top beam). Moreover, the test was performed under displacement control.

The average compressive strength obtained with the compression tests was 2.44 MPa from values between [1.86, 3.03] MPa. Moreover, due to the scatter of results of Young's modulus, different ranges of points were considered for the calculation of the secant stiffness. Considering 0.1*Fmax and 0.33*Fmax, the best fit resulted in an average value of Young's modulus of 3.2 GPa from a range of [1.40, 4.80] GPa.

2.3 Test set-up and procedure

Quasi-static cyclic tests were performed on all specimens according to Applied Technology Council [49] and ASTM E2126-11 [50], and were adapted from the tests previously carried out by Milosevic et al. [47]. The specimens were tested to their in-plane behaviour with an imposed pre-vertical stress of 0.3 MPa, correlated with the actual level of stresses of load-bearing walls in old Lisbon masonry buildings [47] and based on the state of stress measured at the bottom walls of the chapel of the National Palace of Sintra [51]. Thus, the vertical load was applied first during the quasi-static cyclic test with a hydraulic jack.

The boundary conditions were designed as a cantilever system, i.e. the concrete base on which the specimens were built is fixed to the set-up while the top concrete beam is free. This test set-up intends to represent the boundary conditions of masonry piers in ancient buildings with flexible floors and weak spandrels, or even in the case of churches, where no floors exist, and the old wooden rooftops do not restring the rotations at the top. The horizontal load

Table 2 Mechanical characteristics of mortar

Designation	Mortar's age	Average flexural strength (MPa)	c.o.v. (%)	Average compressive strength (MPa)	c.o.v. (%)	Young's modulus* (GPa)
A	28 Days	0.7	7.9	1.9	3.1	5.3–5.8
	4 Months	0.7	7.5	2.2	3.7	–
B	28 Days	2.5	1.9	9.7	3.9	8.7
C	28 Days	4.2	7.2	10.4	4.3	10.5–11.0

*Provided by the manufacturer

Fig. 4 Compression tests to masonry prisms: **a** test set-up, **b** capacity curves

a)   b)
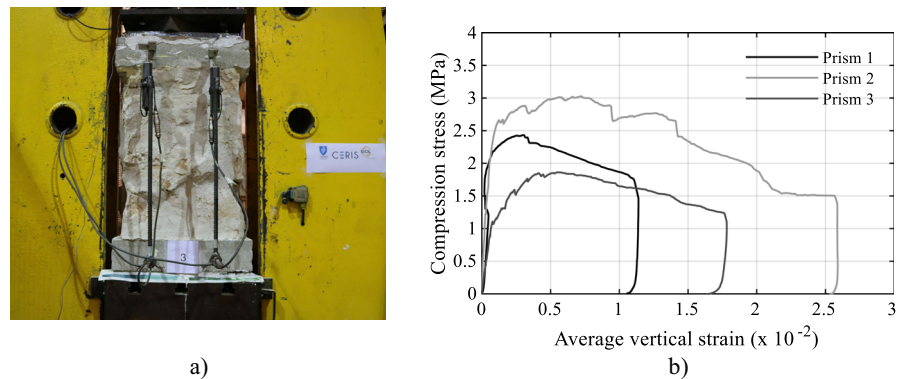
was applied on a steel structure fixed to the concrete beam at the top of the specimen through a mechanical actuator with a load cell of 300 kN capacity. The steel system allowed the proper distribution of the horizontal load along the top face of the specimen, preventing the concentration of stresses on the load application area. The set-up and instrumentation of the quasi-static cyclic test are presented in Fig. 5a and b, respectively.

The loading protocol was divided into two parts. The first one was force-controlled, and the objective was to obtain the elastic branch of the wall´s behaviour. This first part of the loading consisted of four equal increments of load cycles until reaching ¼ of the maximum horizontal force predicted.

The second part of the loading protocol was horizontal displacement controlled through a control wire LVDT attached at mid-height at one end of the top concrete beam and was defined following method B of the standard ASTM E2126-11 [50]. It consisted of five first single fully reversed cycles for the displacements corresponding to 1.25, 2.5, 5, 7.5, and 10% of a predicted ultimate displacement. After, a set of three cycles was applied for each horizontal displacement level, corresponding to 20, 40, 60, 80, 100, and 120%

of the predicted ultimate displacement, with additional increments of 20% until the specimen failure. The loading pattern was revised for each test taking into account updated predicted ultimate displacement values that resulted from the first tested specimens. For the first specimen to be tested, an unreinforced wall, the ultimate displacement predicted to calculate the load pattern was retrieved from [47], which presented a similar type of unreinforced masonry walls but did not account for a deteriorated state of the masonry. Due to the lack of data on this type of wall under quasi-static cyclic tests, it was only possible to find suggestions for drift improvement of stone masonry walls strengthened with injection [52] and a study on one rubble stone wall strengthened with FRCM on one side [36].

The displacement history of horizontal displacement vs. time was obtained with the control horizontal LVDT. Moreover, different LVDTs were placed on the lateral side of each specimen at the bottom, mid-height and top of the masonry panel, with their supports fixed on the stones, as presented in Fig. 5. The LVDTs were placed to obtain both horizontal and vertical displacements, and are identified as TSH if

a)

b)
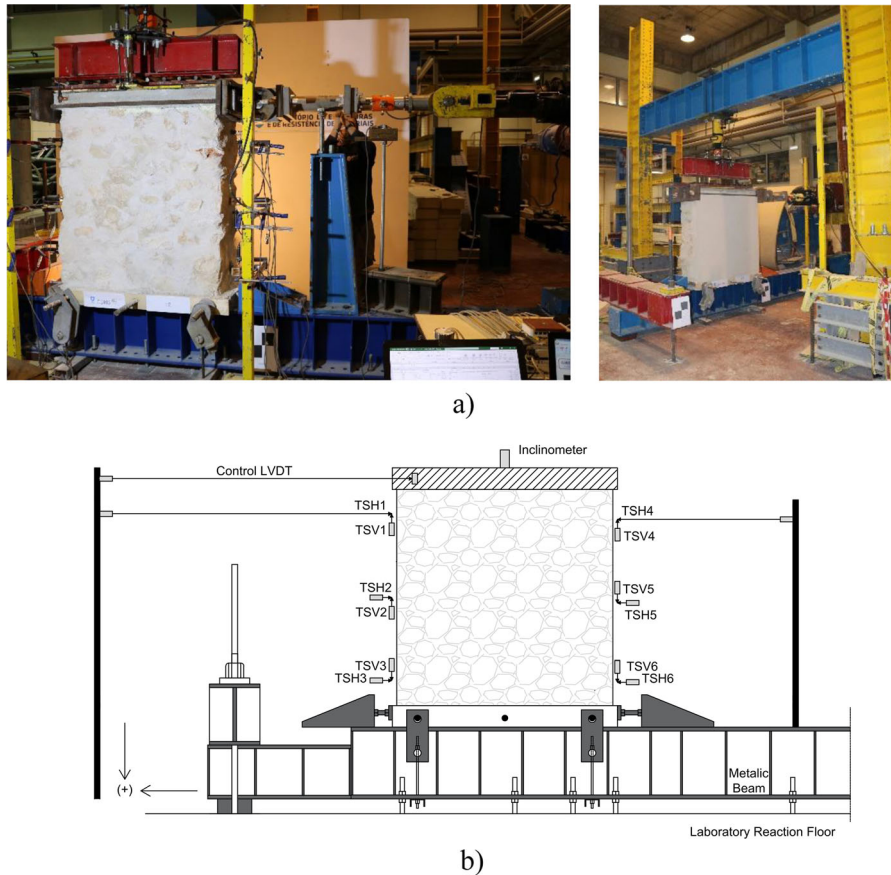
Fig. 5 **a** Set-up and **b** instrumentation of the quasi-static cyclic tests

measuring horizontal displacements, and TSV for vertical displacements, followed by a number that corresponds to a different position on the specimen. To complete this, an inclinometer was placed on the top centre of the concrete beam.

3 Experimental results

### 3.1 Force–displacement hysteresis diagrams and failure modes

Results of the specimens' capacity are presented in terms of force–displacement hysteretic diagrams in Fig. 6, where the envelope curves and the first visible crack are also identified. In the vertical axis, V (kN) represents the horizontal load applied on the top concrete beam corresponding to a cantilever condition. While in the horizontal axis, δ (%) represents the horizontal in-plane drift, which was calculated by dividing the horizontal displacement of the wall between the base and the measuring point of the control LVDT at the concrete beam, by the total height.

Regarding the specimens that presented visible damage at the end of the tests, besides a rigid body rotation, the damage distribution in one of the facades is presented in Fig. 7. For specimen C 1, as the separation of the two leaves of stone occurred, a view of the side facade is also shown. Failure was defined as the point when the specimen achieved a decay of 20% of the horizontal peak load, or when the panel presented such a high level of damage that was on the verge of collapse.

The control specimens (URM 1 and URM 2), both unreinforced, presented a clear decay of strength after reaching their maximum capacity. When the collapse was attained, the specimens were severely damaged

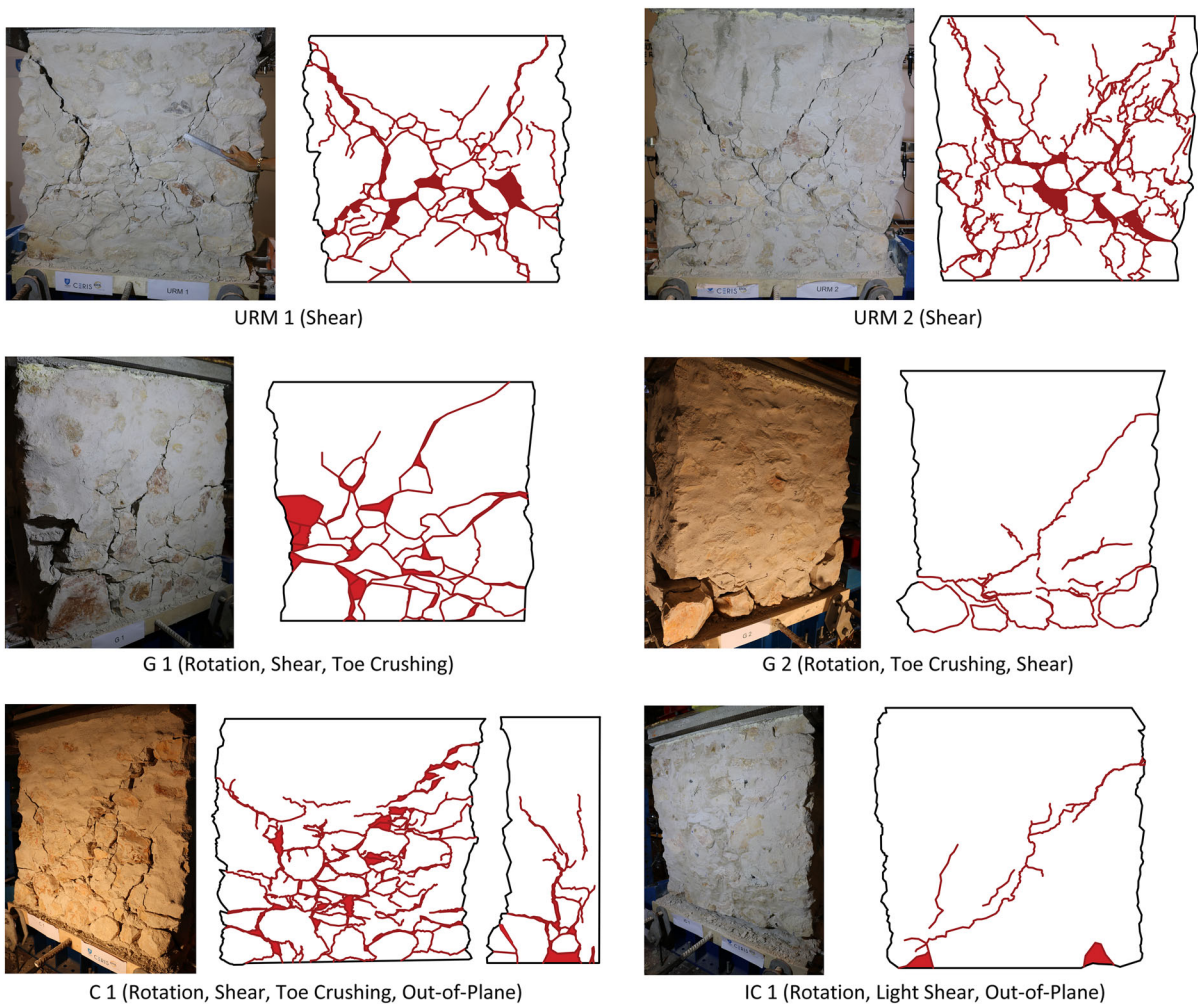**Fig. 6** Force–displacement hysteretic and envelope curves
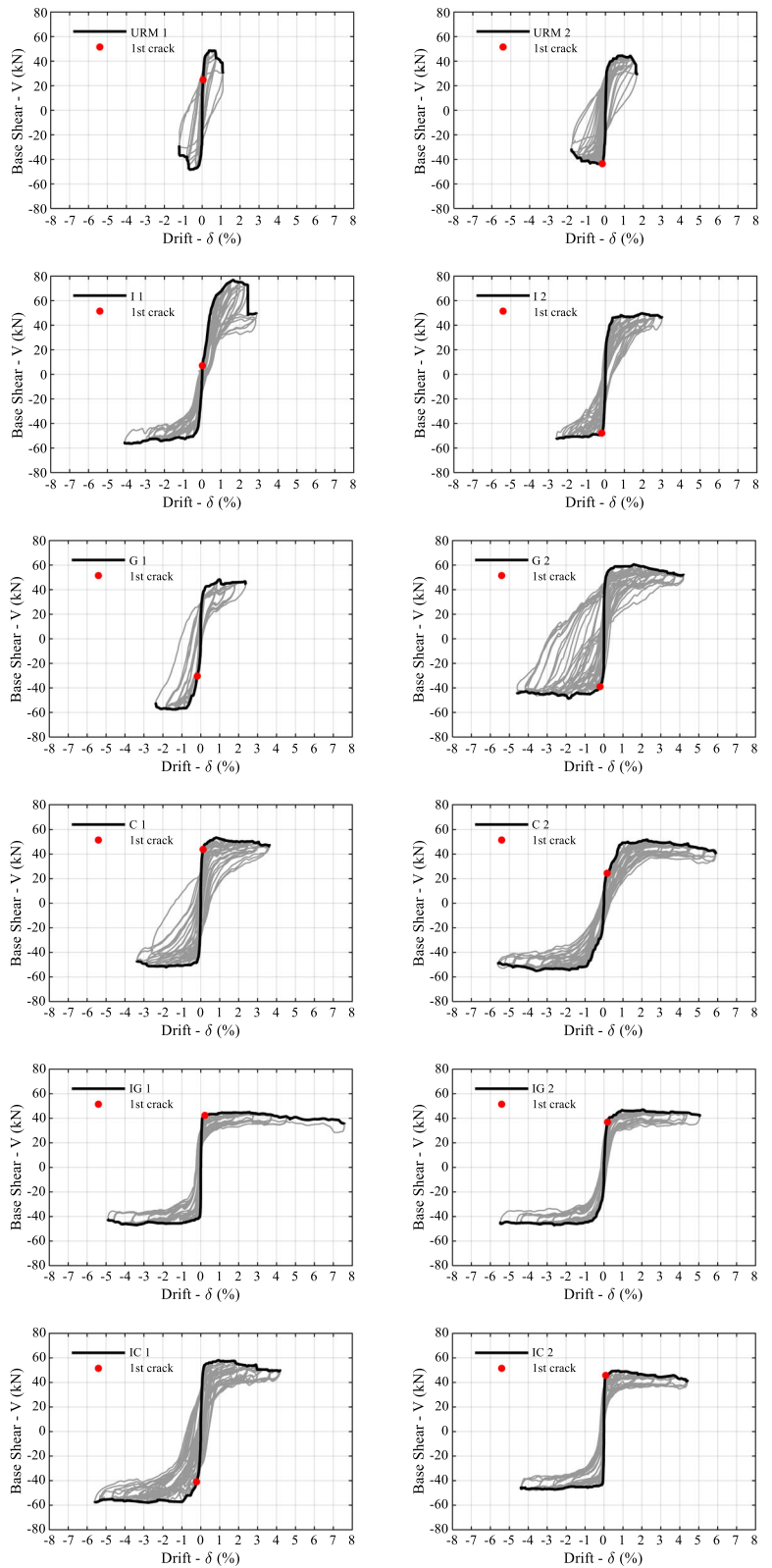
with large diagonal cracks due to shear failure on both sides of the specimens, and a few parts of the specimens were on the verge of detaching from the panel.

It is worth noting that the first visible crack to appear on the strengthened specimens, marked in Fig. 6 with a red dot, corresponded always to the detachment of the masonry panel from the concrete base. Thus, the connection between the masonry panel and the concrete footing proved to be the weakest part of the strengthened specimens, associated with their alteration of behaviour from shear to a rocking mode. This is one of the aspects that would have benefited from a detailed installation of the FRCM system with

fixed ends to the foundation and rooftop, or continuity between storeys, since exploiting the full capacity of the FRCM system would delay the detachment of the wall from the base. When analysing the deformed shapes, it is possible to conclude that the strengthening techniques altered the failure mode of the panels from shear collapse to flexure, mainly defined by rotation, similar to a rigid body behaviour, which sometimes was lately followed by a combination of other types of failure mode. As is typical of the rocking behaviour [53, 54], the strengthened specimens presented hysteretic curves without significant strength deterioration or relevant energy dissipation, showing a typical flag shape.

URM 1 (Shear)

URM 2 (Shear)

G 1 (Rotation, Shear, Toe Crushing)

G 2 (Rotation, Toe Crushing, Shear)

C 1 (Rotation, Shear, Toe Crushing, Out-of-Plane)

IC 1 (Rotation, Light Shear, Out-of-Plane)

Fig. 7 Damage distribution and failure modes at the end of the tests for the damaged specimens (pictures and drawings of front and side facades)

Results of specimen I 1 for positive direction presented a higher strength capacity regarding the other specimens because, during the majority of the cyclic test on specimen I 1, the vertical displacements of the arm that applied the horizontal force to the specimen were restrained, thus imposing a restriction on the rotation of the specimen for the pushing movement. The restraints were removed when this was noticed, significantly lowering the panel strength capacity for this direction to about 65% of its peak load. Thus, reaching the same level of strength as it presents for the negative direction (pull) and as also the other specimen injected with mortar (I 2), represented in the hysteretic curves in Fig. 6. Therefore, the results of specimen I 1 for the positive direction will not be compared with the results of the other specimens further on in this paper. Even so, specimen I 1 presented a rocking behaviour without visible damage.

From the envelope curves in Fig. 8, it is possible to immediately identify a significant positive impact of the retrofitting solutions on the deformation capacity of masonry walls. On the other side, in terms of shear strength, the retrofitting did not cause a significant enhancement since the lateral strength is limited by the rigid body rocking mechanism. It is worth mentioning that the strength experimentally obtained also depends on the contact surface. For these experimental tests, it was used a concrete footing, although in real buildings that should not be the case. Nevertheless, for the specimens in which sliding occurred (I 1, I 2, C 2, IC 1), a range of the maximum value of the friction coefficient was obtained between [0.40, 0.57].

Three specimens (C 1, I 2, IC 1) presented an out-of-plane behaviour due to slight height inclination of the masonry wall, or deviation of the masonry wall regarding the axis of application of the horizontal load, and, in case of the presence of FRCM system, due to the difference of damage state of both sides of the specimen. Even though during the positioning of the specimens in the set-up, attempts were made to rectify the previous issues, the construction of masonry walls is a manual process, and it will be always impossible to eliminate the existing heterogeneities, especially in rubble stone masonry. For specimen C 1, as is visible in Fig. 7, there was even a separation of the two leaves of stone at the base. The poor connection between the two leaves, in this case, is also evident in the extensive damage presented in the unstrengthened facade.

There is a clear distinction in the existing damage in strengthened specimens with mortar injection and without. The specimens with mortar injection presented almost no damage besides the detachment of the panel from the concrete base (Fig. 9), behaving as a rigid body, while the specimens without injection tended to present more damage on the masonry panel, whether it was diagonal cracking, toe crushing, or a combination of both. The cracking was visible only on the facade without the FRCM and the sides except for specimen G 1, the only presenting a crack on the plastered face. Moreover, this difference in behaviour due to the mortar injection is represented in lower energy dissipation of the hysteretic cycles. It is also worth noting, that specimen C 2, presented a rocking behaviour without visible damage, as for the specimens with mortar injection technique. This can be explained by the heterogeneity of the walls, due to the material and manual construction. Moreover, no detachment of the FRP mesh from the masonry panel was noted in any of the specimens.

Table 3 identifies the type of strengthening of each specimen, its corresponding failure mode and the criteria for each specimen that defined its ultimate displacement. For IG 2 and IC 2, it was decided to stop the tests for a displacement similar to the other equivalent specimens, since IG 2 and IC 2 did not present either strength reduction or damage.

3.2 Mechanical parameters obtained from quasi-static cyclic tests

The values obtained from the envelope curves in terms of peak load (V_{max}), ultimate drift (δ_u), and effective stiffness, together with the average values for each type of tested strengthening solution are presented in Table 4. The maximum horizontal force limit given by the horizontal force of a rigid body rocking mechanism (V_{rigid}), which was calculated by the equilibrium of forces and considering the weight of the specimen at its centre of mass, is also presented. In Fig. 10, it is possible to observe the increase in peak load and ultimate drift capacity of the strengthening solutions compared to the unstrengthened specimens. The ultimate drift of each specimen is considered the minimum value between the positive (push) and negative (pull) direction of the horizontal load for which one of the conditions of failure occurred. The effective stiffness was calculated as indicated in
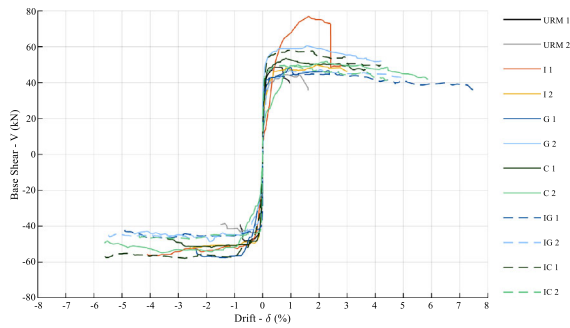
Fig. 8 Envelope curves until the ultimate drift

Fig. 9 Rigid body behaviour of a wall strengthened with injection and G-FRCM system (IG 2), both sides view

Italian Standard [55] for the bilinearization of the envelope curves, as the secant stiffness at $0.7 \times V_{max}$.

As was also observed by Garcia-Ramonda et al. [56], the ultimate drift of the URM walls (1.2% in the current study) is highly underestimated by the building codes [55, 57], which consider a value of 0.5% for the Near Collapse Limit State (failure) of URM walls failing in shear mode. Nonetheless, it is also worth noting that the drift limits depend on several parameters, such as vertical load, boundary conditions, and geometry, whereas in the codes, they only depend on the boundary conditions. As was highlighted by Petry and Beyer [58], the size effect also influences the drift capacity of walls: greater test unit size presents a reduced drift capacity. Thus, the values proposed in the codes cannot be directly compared with the values herein obtained. Regarding drift limit values of strengthened masonry walls with the FRCM system, neither the building codes [55, 57] nor the codes and

guidelines for this retrofitting technique [19, 20, 24, 25] present proposals.

Even though the FRCM solution was only applied on one side of the specimens, not providing confinement to the masonry, it already presents a significant improvement of the ultimate drift, related to the change of failure mode from shear to rocking. It is also worth noting that, the deformation capacity results obtained for the mortar injection technique are not considered representative of this technique and should be considered as a minor of the real behaviour. The ultimate displacement of specimen I 2 was conditioned by out-of-plane collapse, not due to extensive damage or strength decay, and for specimen I 1 the decay of strength was caused by alterations in the boundary conditions, as already explained before.

Regarding the effective stiffness, no relation to the type of strengthening solution was found when compared with the unstrengthened specimens, since, due to the rocking mechanism, the parameter is strongly related to the detachment of the masonry wall from the concrete foundation. The mortar stiffness and the cracks at the connection to the base that might have appeared during the positioning of the specimens in the set-up are thus what influence the equivalent stiffness. Therefore, for the strengthened specimens, the effective stiffness does not represent the effective stiffness of the strengthened masonry material and is of no practical use. In addition, the walls G 1, C 2, and IG 2, the ones that present lower stiffnesses are also the ones in which a crack along the connection of the wall to the base appears for the first imposed horizontal loads.

The cumulative dissipated hysteretic energy was calculated for each cycle and compared with the corresponding maximum absolute value of drift, presented in Fig. 11. It is possible to observe the correlation between the dissipated energy and the type of failure mode of the specimens. Three parabolic trends are identified. URM 1, with a shear collapse, is the specimen that presents the highest dissipated energy when comparing equal values of drift. The specimens that presented rotation followed by diagonal cracks due to shear and toe crushing (G 1, G 2, C 1, I 2, IC 1) present a similar trend of dissipated energy, lower than the URM 1 that was completely damaged by shear. Finally, specimens like IG 1, IG 2, IC 2, and C 2, with mostly only rocking behaviour and no visible

Table 3 Identification of failure modes and the criteria to define the ultimate displacement

Specimen	Strengthening	Dominant failure mode	Final damage pattern	Ultimate displacement
URM 1	No	Shear	Diagonal cracking	20% strength decay
URM 2	No	Shear	Diagonal cracking	20% strength decay
I 1	Injection	Flexure	Rotation, sliding	20% strength decay
I 2	Injection	Flexure	Rotation, sliding, out-of-plane	Local mechanism
G 1	GFRCM	Hybrid (dominated by flexure)	Rotation, diagonal cracking, toe crushing	Local mechanism
G 2	GFRCM	Hybrid (dominated by flexure)	Rotation, toe crushing, light diagonal cracking	20% strength decay
C 1	CFRCM	Hybrid (dominated by flexure)	Rotation, diagonal cracking, toe crushing, out-of-plane	Local mechanism
C 2	CFRCM	Hybrid (dominated by flexure and sliding)	Rotation, sliding	20% strength decay
IG 1	Injection + GFRCM	Flexure	Rotation, light toe crushing	20% strength decay
IG 2	Injection + GFRCM	Flexure	Rotation	No criterion
IC 1	Injection + CFRCM	Hybrid (dominated by flexure and sliding)	Rotation, sliding, light diagonal cracking, out-of-plane	Local mechanism
IC 2	Injection + CFRCM	Flexure	Rotation	No criterion

Table 4 Values of peak load, drift at failure, and effective stiffness

| Specimen	Peak load (kN)			V_{rigid} (kN)	Drift at failure (%)				Effective stiffness (kN/mm)		
	+	−	Mean		+	−	δ_u	Mean	+	−	Mean
URM 1	49.1	48.3	46.4	67	1.0	0.8	0.8	1.2	26.2	53.7	37.6
URM 2	44.5	43.7		70	1.6	1.7	1.6		32.9	37.4	
I 1	–	56.4	52.8	73	–	4.1	4.1	3.4	–	16.9	17.4
I 2	49.7	52.4		78	3.0	2.6	2.6		17.4	34.3	
G 1	48.3	57.5	53.8	75	2.4	2.4	2.4	3.3	32.7	10.4	38.9
G 2	60.6	48.7		76	4.2	4.6	4.2		83.2	29.1	
C 1	53.4	52.1	53.1	76	3.6	3.4	3.4	4.7	45.4	39.2	23.7
C 2	51.8	55.0		72	5.9	5.6	5.9		4.8	5.4	
IG 1	45.0	46.9	46.5	74	7.5	4.9	7.5	6.3	43.4	178.3	61.9
IG 2	47.1	47.1		73	5.1	5.5	5.1		16.3	9.6	
IC 1	58.0	57.9	53.4	77	4.2	5.6	4.2	4.3	39.2	14.5	50.3
IC 2	49.6	48.0		71	4.4	4.4	4.4		88.5	59.0	
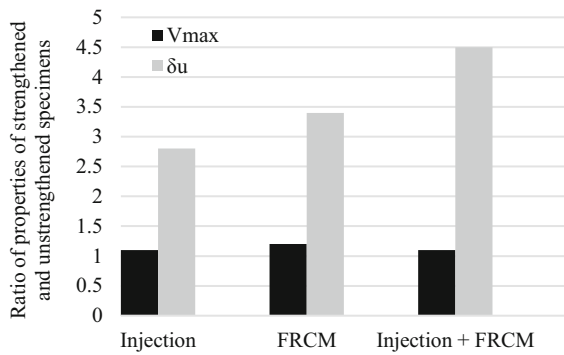
Fig. 10 Ratio of properties of strengthened to unstrengthened specimens

damage, present a trend of low dissipated energy, as it is common in this type of failure mode.

A collection of data on the improvement of mechanical properties of masonry strengthened with mortar injection or FRCM systems is presented in Table 5. The available cyclic tests on rubble stone walls strengthened with the herein studied retrofitting techniques were gathered and presented. Moreover, to join information on strengthened walls with shear failure, focusing on retrofitting with the FRCM system, for which does not exist so much data as for injection technique, relevant studies of diagonal compression tests on rubble stone masonry were also collected. It is worth mentioning that for the application of FRCM systems on masonry, even though studies with cyclic tests are scarce, it is possible to obtain some data, mostly for brick masonry [26]. However, for masonry walls strengthened simultaneously with mortar injection and the FRCM system the authors could only find the diagonal compression tests carried out by Ferretti et al. [34]. For values signed with an *, this means that the value presented is a minor of the real capacity of the wall since due to some constrain the test had to be stopped before attaining the in-plane failure of the wall. As it is possible to observe, in general, the results herein obtained are in accordance with the ones presented in the literature.

Regarding the values for strengthening with FRCM systems, the increase in terms of peak load is similar; however, for drift limits, as the failure modes were not the same, different values are proposed. As mentioned by Vanin et al. [52], the strengthening solutions present more influence on the deformation capacity if the failure mode changes from shear to flexure.
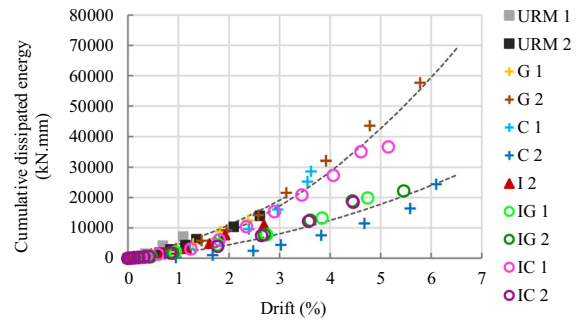
Fig. 11 Cumulative dissipated energy (kN mm)

For walls strengthened simultaneously with injection and FRCM system on one side of the wall, no other results from cyclic tests were found in the literature. Therefore, the results herein presented are the only ones proposed so far.

4 Conclusions

This paper presents a first step towards the study of strengthening techniques with mortar injection and FRCM systems applied to rubble limestone with hydraulic mortar masonry walls, typical of historical monumental and residential buildings of the southern European countries, more specifically Lisbon, Portugal. The FRCM systems herein studied were applied only to one face of the specimens, as it happens so commonly in reality, in which one side is of difficult access, or due to the presence of architectural and decorative elements. Additionally, the FRCM system was defined with an anchoring system to the masonry substrate, but no mechanical devices were applied to fix the ends of the mesh to the foundation or top beam. This limitation is studied here since it represents the reality of heritage buildings when it is not often possible to guarantee the continuity of the solution to the foundation or the rooftop.

The experimental campaign consists of quasi-static cyclic tests on both strengthened and unstrengthened rubble stone specimens. The specimens are studied for the boundary condition of a cantilever, representative of buildings with weak spandrels and flexible floors. Moreover, the masonry specimens are built on a concrete base with a poor connection mainly based on the mortar's resistance. Increased ultimate drift and strength values due to the application of these

Table 5 Comparison of mechanical properties between strengthened and unstrengthened masonry specimens—literature review

Intervention	Failure mode of specimens		Pier dimensions L × H × T (mm)	Axial stress level (MPa)	Type of test	Boundary conditions/Load scheme	Ratio of properties of strengthened and unstrengthened specimens		Type of masonry	Mesh	Reference
	Unstrengthened	Strengthened					Peak load	Ultimate Horizontal Drift			
Injection	Flex	Flex	800 × 1000 × 330	1.0/1.25	Cyclic	Cantilever	1.3/1.4	2.9	Rubble Stone	–	Silva [59]
	Shear	Flex	1000 × 1200 × 500	1.0/1.25	Cyclic	Cantilever	1.5/2.0	5.3	Rubble Stone	–	Silva [59]
FRCM (one side)	Shear	Hybrid (dominated by flexure)	**1200 × 1200 × 400**	**0.3**	**Cyclic**	**Cantilever**	**1.1**	**2.8[a]**	**Rubble Stone**	**Glass/Carbon**	**Current Study**
			1200 × 1200 × 400	**0.3**	**Cyclic**	**Cantilever**	**1.2**	**3.4**	**Rubble Stone**	**Glass/Carbon**	**Current Study**
		OOP bending	1500 × 2000 × 350	0.9	Cyclic	Double Fixed	1.2	2.6[a]	Rubble Stone	Glass	Gattesco et al. [36]
		Shear	1200 × 1200 × 240	–	DC	Load-unload	1.9	–	Rubble Stone	Glass	Castori et al. [33]
FRCM (two sides)	Shear	Shear	1270 × 1270 × 310	0.3	Cyclic	Double Fixed	1.3	–	Brick	Low-density Basalt	García-Ramonda et al. [60]
			1000 × 1500 × 500	0.3	Cyclic	Double Fixed	4.2	1.5	Rubble Stone	Glass	Tomaževič et al. [38]
			1200 × 1200 × 240	–	DC	Load-unload	2.7	–	Rubble Stone	Glass	Castori et al. [33]
			1200 × 1200 × 540	–	DC	Load-unload	2.8	–	Rubble Stone	Glass	Angiolilli et al. [61]
		Connector's failure	1500 × 2000 × 350	0.9	Cyclic	Double Fixed	1.4	1.9	Rubble Stone	Glass	Gattesco et al. [36]
Injection + FRCM (one side)	Flex	Flex	1250 × 1560 × 400	0.2/0.4	Cyclic	Cantilever	1.7/1.6	–	Rubble Stone[b]	Carbon	Guerreiro et al. [37]
			1120 × 1200 × 95	0.3	Cyclic	Cantilever	1.2	4.5	Stones	Basalt	Papanicolaou et al. [40]
		Flex	**1200 × 1200 × 400**	**0.3**	**Cyclic**	**Cantilever**	**1.1**	**4.5**	**Rubble Stone**	**Glass/Carbon**	**Current Study**
Injection + FRCM (two sides)	Shear	Shear	1300 × 1300 × 480	–	DC	Monotonic	6.5	–	Rubble Stone	Basalt	Ferretti et al. [34]

[a] Minor of the real ratio; [b] "Equivalent" homogeneous material, replicating the mechanical characteristics of rubble stone; DC diagonal compression

strengthening techniques are observed, indicating the usability of these retrofitting solutions for the design of practical cases. Both techniques prove to be effective by altering the shear collapse of a masonry specimen to one controlled by flexure (mainly rocking). Thus, the increase in shear strength is not completely exploited as the lateral response is switched to in-plane rocking with a significant increase in displacement capacity. Values of ultimate lateral drift of 3.4, 4.0, and 5.3% are observed for walls with the injection of mortar, FRCM system on one facade, and simultaneously injection and FRCM system, respectively.

More comments are made in this paper considering the behaviour of the different solutions, in terms of capacity curves, damage patterns, and energy dissipation. It is worth noting the clear distinction in the damage presented by walls with and without the injection of mortar. For the first, almost no damage is present, and the walls present mainly a rigid body rocking behaviour. Joining simultaneously the injection and FRCM system allowed the piers to present a higher displacement capacity with lower strength degradation (never reaching ultimate displacement due to strength decay) and without damage to the masonry. Even so, the benefits of combining the two techniques are almost negligible for the rocking mechanism.

Besides the wide investigations on assessing the effectiveness of the FRCM system for increasing the shear capacity of masonry walls, there is still a gap in the study of their in-plane cyclic capacities, especially for rubble stones. Further experimental campaigns with cyclic tests would be required for rubble stone masonry, considering different aspect ratios, boundary conditions, and fabric reinforcements, among others. The results of these additional tests would enable drawing more general conclusions on the benefit of FRCM regarding the in-plane horizontal drift capacity of masonry piers, particularly in the case of shear failure. Even though more experimental tests should be performed to increase the representativeness of results, the values herein obtained represent a reference start for the design of strengthening solutions in historical buildings with rubble limestone and hydraulic mortar masonry walls.

In this study, the benefit of the two meshes (glass and carbon fibres) was similar, changing the failure mode from shear to rocking, whereas the benefit of the carbon mesh was not fully exploited due to the static

scheme, boundary conditions, aspect ratio, and vertical load. Therefore, to understand which type of material would bring more advantages to the FRCM system on masonry walls, a study with connections to fix the FRP mesh to the concrete base and different boundary conditions in which another type of mechanism prevails must be carried out. It is expected that for the same test set-up, connecting the FRCM system to the masonry pier ends may not prevent the rocking behaviour; however, it should result in greater effective stiffness by delaying the debonding of the wall from the concrete base, higher lateral strength of the pier, and higher dissipative energy.

References

1. Guerreiro L, Azevedo J, Proença J, Bento R, Lopes M (2000) Damage in ancient churches during the 9th of July 1998 Azores earthquake. In: Proceedings of the XII World Conference on Earthquake Engineering, Auckland.

2. D'Ayala DF, Paganoni S (2010) Assessment and analysis of damage in L'Aquila historic city centre after 6th April 2009. Bull Earthq Eng 9(1):81–104. https://doi.org/10.1007/s10518-010-9224-4

3. Penna A, Calderini C, Sorrentino L, Carocci CF, Cescatti E, Sisti R, Borri A, Modena C, Prota A. (2019). Damage to churches in the 2016 central Italy earthquakes. Bull Earthquake Eng 17(10):5763–5790. https://doi.org/10.1007/s10518-019-00594-4

4. Calderoni B, Cordasco EA, Del Zoppo M, Prota A (2020) Damage assessment of modern masonry buildings after the L'Aquila earthquake. Bull Earthq Eng 18(5):2275–2301. https://doi.org/10.1007/s10518-020-00784-5

5. Milosevic J, Gago AS, Lopes M, Bento R (2013) Experimental assessment of shear strength parameters on rubble stone masonry specimens. Constr Build Mater 47:1372–1380. https://doi.org/10.1016/j.conbuildmat.2013.06.036

6. Silva B, Dalla Benetta M, da Porto F, Modena C (2014) Experimental assessment of in-plane behaviour of three-leaf stone masonry walls. Constr Build Mater 53:149–161. https://doi.org/10.1016/j.conbuildmat.2013.11.084

7. Corradi M, Borri A (2018) A database of the structural behavior of masonry in shear. Bull Earthq Eng 16(9):3905–3930. https://doi.org/10.1007/s10518-018-0328-6

8. Boschi S, Galano L, Vignoli A (2019) Mechanical characterisation of Tuscany masonry typologies by in situ tests. Bull Earthq Eng 17(1):413–438. https://doi.org/10.1007/s10518-018-0451-4

9. Sorrentino L, da Porto F, Magenes G, Penna A (2018) Seismic behaviour of ordinary masonry buildings during the 2016 central Italy earthquakes. Bull Earthq Eng 17:5583–5607. https://doi.org/10.1007/s10518-018-0370-4

10. Augenti N, Parisi F (2010) Learning from construction failures due to the 2009 L'Aquila, Italy, earthquake. J Performance Constructed Facilities 24(6):536–555. https://doi.org/10.1061/(ASCE)CF.1943-5509.0000122

11. Decanini L, De Sortis A, Goretti A, Langenbach R, Mollaioli F, Rasulo A (2004) Performance of masonry buildings during the 2002 Molise, Italy, earthquake. Earthq Spectra 20(S1):S191–S220. https://doi.org/10.1193/1.1765106

12. ICOMOS/ISCARSAH Committee (2003). Recommendations for the analysis, conservation and structural restoration of architectural heritage. ICOMOS International Committee for the Analysis and Restoration of Structures of Architectural Heritage.

13. Oliveira DV, Silva RA, Garbin E, Lourenço PB (2012) Strengthening of three-leaf stone masonry walls: an experimental research. Mater Struct/Materiaux et Constructions 45:1259–1276. https://doi.org/10.1617/s11527-012-9832-3

14. Binda L, Modena C, Baronio G, Abbaneo S (1997) Repair and investigation techniques for stone masonry walls. Constr Build Mater 11(3):133–142. https://doi.org/10.1016/s0950-0618(97)00031-7

15. Miranda L, Milosevic J, Bento R (2017) Cyclic behaviour of stone masonry walls strengthened by grout injection. Mater Struct/Materiaux et Constructions 50(1):1–17. https://doi.org/10.1617/s11527-016-0911-8

16. Vintzileou E, Tassios TP (1995) Three-leaf stone masonry strengthened by injecting cement grouts. J Struct Eng 121(5). https://doi.org/10.1061/(ASCE)0733-9445(1995)121:5(848)

17. Valluzzi MR, da Porto F, Modena C (2004) Behavior and modeling of strengthened three-leaf stone masonry walls. Mater Struct 37(3):184–192. https://doi.org/10.1007/bf02481618

18. Penazzi D, Valluzzi MR, Cardani G, Binda L, Baronio G, Modena C (2000) Behaviour of Historic Masonry buildings in seisimic areas: lessons learned from the Umbria-Marche Earthquake. In: Proceedings of 12th International Brick/Block Masonry Conference. Madrid, Spain.

19. AC434-13 (2013) Acceptance criteria for masonry and concrete strengthening using fabric-reinforced cementitious matrix (FRCM) composite systems. ICC Evaluation Service.

20. CNR-DT 215/2018 (2018) Guide for the design and construction of externally bonded FRP systems for strengthening existing structures. Rome: CNR—Advisory Committee on Technical Recommendations for Construction.

21. CSLP (Consiglio Superiore del Lavori Pubblici) (2018) Guideline for the identification, qualification and acceptance control of Fibre Reinforced Cementitious Matrix (FRCM) used for the structural consolidation of existing constructions. Rome: CSLP 01/01/2019, n.1.

22. CSLP (Consiglio Superiore del Lavori Pubblici) (2019a) Guidelines for design, execution and maintenance of strengthening interventions by means of Fibre Reinforced Cementitious Matrix (FRCM) systems. Rome: CSLP 03/12/2019, n. 627.

23. CSLP (Consiglio Superiore del Lavori Pubblici) (2019b) Guideline for the identification, qualification and acceptance control of fibre-reinforced composites systems with preformed mesh, based on polymer matrix, used for the structural consolidation of existing constructions with the CRM (Composite Reinforced Mortar) technique. Rome: CSLP 29/05/2019, n. 292.

24. Technical Committee RILEM, 232-TDT (2016) Recommendation of RILEM TC 232-TDT: test methods and design of textile reinforced concrete - Uniaxial tensile test: test method to determine the load bearing behavior of tensile specimens made of textile reinforced concrete. Mater Struct 49(12):4923–4927. https://doi.org/10.1617/s11527-016-0839-z

25. ACI Committee 549.6R-20 (2020) Guide to design and construction of externally bonded fabric-reinforced cementitious matrix (FRCM) and steel-reinforced grout (SRG) systems for repair and strengthening masonry structures, ACI Webinar Notes. American Concrete Institute, Farmington Hills

26. Boem I (2022) Masonry elements strengthened with TRM: areview of experimental. Des Numer Methods Build 12:1307. https://doi.org/10.3390/buildings12091307

27. Balsamo A, Iovinella I, Morandini G, Maddaloni G (2014) Experimental Investigation on IMG masonry reinforcement. In IABSE Reports. IABSE Symposium, Madrid 2014: Engineering for Progress, Nature and People, vol 102, pp 253–260. International Association for Bridge and Structural Engineering (IABSE). https://doi.org/10.2749/222137814814027594

28. Ferretti F, Incerti A, Ferracuti B, Mazzotti C (2017) FRCM strengthened masonry panels: the role of mechanical anchorages and symmetric layouts. Key Eng Mater 747:334–341. https://doi.org/10.4028/www.scientific.net/KEM.747.334

29. Guerrini G, Bruggi A, Urso S, Quaini M, Penna A (2021) Diagonal compression tests on stone masonry wallettes jacketed with different techniques. In: Murico7—Mechanics of masonry structures strengthened with composite materials.

30. Gams M, Tomaževič M, Berset T (2017) Seismic strengthening of brick masonry by composite coatings: an experimental study. Bull Earthq Eng 15:4269–4298. https://doi.org/10.1007/s10518-017-0136-4

31. Türkmen ÖS, De Vries BT, Wijte SNM, Vermeltfoort AT (2019) Quasi-static cyclic in-plane testing of masonry walls strengthened with a single-sided fabric-reinforced cementitious matrix overlay and flexible anchorage. J Build Pathol Rehab 4(1):1–22

32. Corradi M, Borri A, Castori G, Sisti R (2014) Shear strengthening of wall panels through jacketing with cement mortar reinforced by GFRP grids. Compos B Eng 64:33–42. https://doi.org/10.1016/j.compositesb.2014.03.022

33. Castori G, Corradi M, Sperazini E (2021) Full size testing and detailed micro-modeling of the in-plane behavior of FRCM–reinforced masonry. Construct Build Mater 299:124276. https://doi.org/10.1016/j.conbuildmat.2021.124276

34. Ferretti F, Incerti A, Mazzotti C (2021) Efficiency of strengthening interventions on stone masonry panels through Grout injection and FRCM. Key Eng Mater 916:352–360. https://doi.org/10.4028/p-7i08im

35. Del Zoppo M, Di Ludovico M, Balsamo A, Prota A (2020) Diagonal compression testing of masonry panels with irregular texture strengthened with inorganic composites. Mater Struct 53(4):1–17. https://doi.org/10.1617/s11527-020-01539-z

36. Gattesco N, Amadio C, Bedon C (2015) Experimental and numerical study on the shear behavior of stone masonry walls strengthened with GFRP reinforced mortar coating and steel-cord reinforced repointing. Eng Struct. https://doi.org/10.1016/j.engstruct.2015.02.024

37. Guerreiro J, Proença J, Ferreira JG, Gago A (2018) Experimental characterization of in-plane behaviour of old masonry walls strengthened through the addition of CFRP reinforced render. Compos B Eng 148:14–26. https://doi.org/10.1016/j.compositesb.2018.04.045

38. Tomaževič M, Gams M, Berset T (2015) Strengthening of stone masonry walls with composite reinforced coatings. Bull Earthq Eng 13(7):2003–2027. https://doi.org/10.1007/s10518-014-9697-7

39. Papanicolaou CG, Triantafillou TC, Karlos K, Papathanasiou M (2007) Textile-reinforced mortar (TRM) versus FRP as strengthening material of URM walls: In-plane cyclic loading. Mater Struct 40:1081–1097. https://doi.org/10.1617/s11527-006-9207-8

40. Papanicolaou CG, Triantafillou TC, Lekka M (2011) Externally bonded grids as strengthening and seismic retrofitting materials of masonry panels. Constr Build Mater 25:504–514. https://doi.org/10.1016/j.conbuildmat.2010.07.018

41. Messali F, Metelli G, Plizzari G (2017) Experimental results on the retrofitting of hollow brick masonry walls with reinforced high performance mortar coatings. Constr Build Mater 141:619–630. https://doi.org/10.1016/j.conbuildmat.2017.03.112

42. Mercedes L, Bernat-Maso E, Gil L (2020) In-plane cyclic loading of masonry walls strengthened by vegetal-fabric-reinforced cementitious matrix (FRCM) composites. Eng Struct 221:111097. https://doi.org/10.1016/j.engstruct.2020.111097

43. D'Ambrisi A, Mezzi M, Caporale A (2013) Experimental investigation on polymeric net-RCM reinforced masonry panels. Compos Struct 105:207–215. https://doi.org/10.1016/j.compstruct.2013.05.017

44. Petry S, Beyer K (2014) Cyclic test data of six unreinforced masonry walls with different boundary conditions. Earthq Spectra 31(4):2459. https://doi.org/10.1193/101513EQS269

45. CEN (2006) EN 1926: Natural stone test methods—determination of compressive strength. Brussels: European Committee for Standardization. Retrieved from www.iso.org/iso/foreword.html.

46. Moura AC, Carvalho C, Almeida IA, Saúde JG, Ramos JF, Augusto JP, et al. (2007) Mármores e calcários ornamentais de Portugal/Ornamental marble and limestone from Portugal (in Portuguese). (A. C. Moura, Ed.)

47. Milosevic J, Lopes M, Gago AS, Bento R (2015) In-plane seismic response of rubble stone masonry specimens by means of static cyclic tests. Constr Build Mater 82:9–19. https://doi.org/10.1016/j.conbuildmat.2015.02.018

48. CEN (2019) EN 1015-11: Methods of test for mortar for masonry - Part 11: Determination of flexural and compressive strength of hardened mortar. European Committee for Standardization. Retrieved from www.iso.org/iso/foreword.html, Brussels

49. Applied Technology Council (2007) Interim testing protocols for determining the seismic performance characteristics of structural and Nnonstructural components— FEMA 461.

50. American Society for Testing and Materials—ASTM (2018) ASTM E2126-11: Standard Test Methods for Cyclic (Reversed) Load Test for Shear Resistance of Vertical Elements of the Lateral Force Resisting Systems forBuildings, ASTM International (Vol 1). United States. https://doi.org/10.1520/E2126

51. Ponte M, Bento R, Costa AA, Quelhas B, Guedes JM, Ilharco T, Lopes V (2021) Reduction of earthquake risk of the National Palace of Sintra in Portugal: The palatine chapel. Int J Disaster Risk Reduct 60. https://doi.org/10.1016/j.ijdrr.2021.102172

52. Vanin F, Zaganelli D, Penna A, Beyer K (2017) Estimates for the stiffness, strength and drift capacity of stone masonry walls based on 123 quasi-static cyclic tests reported in the literature. Bull Earthq Eng 15(12):5435–5479. https://doi.org/10.1007/s10518-017-0188-5

53. Magenes G, Calvi GM (1997) In-plane seismic response of brick masonry walls. Earthquake Eng Struct Dynam 26(11):1091–1112. https://doi.org/10.1002/(SICI)1096-9845(199711)26:11%3c1091::AID-EQE693%3e3.0.CO;2-6

54. Magenes G, Morandi P, Penna A (2008) In-plane cyclic tests of calcium silicate masonry walls. In: 12th

International Brick/Block Masonry Conference. Sydney, Australia 18-20/2/2008.

55. Ministero delle Infrastrutture e dei Trasporti. (2018). CIRCOLARE n.35 del 21 gennaio 2019. Istruzioni per l'applicazione dell'«Aggiornamento delle "Norme tecniche per le costruzioni"» di cui al decreto ministeriale 17 gennaio 2018. (Italian Guideline). *Supplemento Ordinario Alla "Gazzetta Ufficiale,, n. 35 Del 11 Febbraio 2019 - Serie Generale*, 337. Retrieved from https://www.gazzettaufficiale.it/eli/gu/2019/02/11/35/so/5/sg/pdf

56. Garcia-Ramonda L, Pelà L, Roca P, Camata G (2022) Cyclic shear-compression testing of brick masonry walls repaired and retrofitted with basalt textile reinforced mortar. Composite Struct 283. https://doi.org/10.1016/j.compstruct.2021.115068

57. CEN (2017) EN 1998-3: Eurocode 8 - Design of structures for earthquake resistance. Part 3: Assessment and retrofitting of buildings (EC8–3). Brussels: European Committee for Standardization. Retrieved from www.iso.org/iso/foreword.html

58. Petry S, Beyer K (2014) Influence of boundary conditions and size effect on the drift capacity of URM walls. Eng Struct 65:76–88. https://doi.org/10.1016/j.engstruct.2014.01.048

59. Silva B (2012) Diagnosis and strengthening of historical masonry structures: numerical and experimental analysis. PhD thesis, University of Padova, Italy.

60. Garcia-Ramonda L, Pelà L, Roca P, Camata G (2022) Experimental and Numerical Analysis of the Cyclic In-Plane Behaviour of Retrofitted Masonry Walls. In: 9th Euro-American Congress on Construction Pathology, Rehabilitation Technology and Heritage Management (REHABEND 2022). Granada, Spain, 13–16/09/2022.

61. Angiolilli M, Gregori A, Cattari S (2021) Performance of fiber reinforced Mortar coating for irregular stone masonry: experimental and analytical investigations. Const Build Mater 294:123508. https://doi.org/10.1016/j.conbuildmat.2021.123508